J Nanopart Res (2021) 23: 36
https://doi.org/10.1007/s11051-020-05106-z

RESEARCH PAPER

Enhanced antibacterial activity of decahedral silver nanoparticles

Sharda Bharti · Soumyo Mukherji · Suparna Mukherji

Received: 23 April 2020 / Accepted: 25 November 2020 / Published online: 17 January 2021

Abstract The size and shape of silver nanoparticles (AgNPs) can potentially influence their antibacterial activity. In this study, a photochemical approach was adopted for the synthesis of decahedral AgNPs and their antibacterial activity was tested and compared against that of spherical AgNPs of similar size synthesized using the chemical reduction approach. The UV–vis spectra indicated the synthesis of decahedral AgNPs with a localized surface plasmon resonance (LSPR) peak at 502 nm. The spherical AgNPs exhibited the LSPR peak at 416 nm. Analysis of field emission gun-transmission electron microscopy (FEG-TEM) micrographs demonstrated the average diameter of decahedral silver nanoparticles as 52.1 ± 5.7 nm with side length as 33.2 ± 3.1 nm. In contrast, the average size of spherical AgNPs was 44.2 ± 6.3 nm. The decahedral AgNPs demonstrated ten times higher bactericidal activity as compared to the spherical AgNPs across all the bacterial strains tested. The minimum inhibitory concentration (MIC) for decahedral AgNPs was in the range of 4–8 μg/ml for all the four bacterial strains tested, whereas, for spherical nanoparticles of comparable size, the MIC was in the range of 40–80 μg/ml. The minimum bactericidal concentration (MBC) for decahedral AgNPs was in the range of 6–10 μg/ml. At the same time, spherical AgNPs of comparable size exhibited MBC in the range of 60–100 μg/ml for the four bacterial strains. In terms of bactericidal effect, *Escherichia coli* MTCC 443 was found as the most sensitive strain, while in terms of growth inhibition, *Bacillus subtilis* was the most sensitive strain. *Staphylococcus aureus* NCIM 5021 was the most resistant among the tested bacterial strains.

Keywords Antibacterial activity · Minimum bactericidal concentration · Minimum inhibitory concentration · Decahedral silver nanoparticles · Localized surface plasmon resonance

S. Bharti · S. Mukherji (✉)
Environmental Science and Engineering Department, IIT Bombay, Mumbai 400076, India
e-mail: mitras@iitb.ac.in

S. Mukherji
Department of Bioscience and Bioengineering, IIT Bombay, Mumbai 400076, India

Introduction

The occurrence of a variety of pathogenic microorganisms including bacteria, fungi, and viruses is reported in potable water (Ashbolt 2015). The contamination of water bodies by such waterborne pathogens is a major concern throughout the world as these microorganisms have been linked to various diseases (Pandey et al. 2014). Among various bacterial strains in potable water, classic examples of waterborne enteric pathogens include *Salmonella enterica*, *Vibrio cholerae* (serogroups O1 and O139), and *Shigella* spp. (Pandey et al. 2014). Moreover, fecal contamination of potable water may also cause the spread of various pathogenic strains, such as *Escherichia coli*, *Staphylococcus aureus*, *Bacillus subtilis*, *Pseudomonas aeruginosa*, *Helicobacter*, *Salmonella*, and *Yersinia* (Ashbolt 2015). The formation of

biofilms in the drinking water distribution system (DWDS) further impedes the efforts to control and eradicate these microbes. Multidrug-resistant bacterial strains and strains existing in biofilms are resistant to various antibiotics (Ito et al. 2009; Araújo et al. 2011). A large population of persisters may also exist in the DWDS (Keren et al. 2004). These persisters neither grow in the presence of antibiotics nor die in their presence due to the development of specific resistance mechanisms. In such case, AgNPs may play a vital role compared to the conventional antibiotics as they kill a diverse range of pathogenic microorganisms and resistance to them has not been reported yet (Chudasama et al. 2009; Rai et al. 2009). This may be attributed to the fact that AgNPs act via multiple mechanisms by acting on multiple targets within a microorganism. Hence, it is difficult for microorganisms to develop resistance against AgNPs, as opposed to the conventional antibiotics (Chudasama et al. 2009). The oligotrophic properties and broad-spectrum killing caused by AgNPs have encouraged their use for inactivation of diverse microbial strains including multidrug-resistant (MDR) strains (Silvestry-rodriguez et al. 2007; Agnihotri et al. 2013; Yang et al. 2013; Mlalila et al. 2016). A number of mechanisms have been reported for antimicrobial activity of AgNPs such as disruption of the bacterial cell membrane, interference in the respiratory electron transport chain by binding to functional proteins and enzymes, hindering the process of DNA replication, and formation of reactive oxygen species (ROS) (Sondi and Salopek-Sondi 2004; Pal et al. 2007; Yang et al. 2013; Bharti et al. 2015; Franci et al. 2015).

The antimicrobial activities of AgNPs are known to be dependent on a number of factors; however, the shape and size of AgNPs significantly affect their efficacy (Mukherji et al. 2018). Hence, some of the recent studies have specifically focused on the antimicrobial activity of size- and shape-controlled AgNPs. The chemical synthesis approach based on reduction of Ag^+ ions has been widely used for the synthesis of spherical AgNPs (Guzmán et al. 2009; Agnihotri et al. 2014; Iravani et al. 2014). Its advantages include its simplicity, homogeneity in terms of shape and size, stability of the products, and the ease of process scale-up (Mlalila et al. 2016). However, nanoparticles with sharp edges, i.e., anisotropic nanoparticles, have shown enhanced activity compared to spherical nanoparticles (Pal et al. 2007; Navaladian et al. 2008; Goyal et al. 2017; Murph et al. 2017). Pal et al. (2007) demonstrated higher antimicrobial efficacy for the truncated triangular silver nanoplates compared to that of rod-shaped and spherical nanoparticles. It has been proposed that nanoparticles with sharp edges exhibit higher activity. It has been demonstrated that the surface charge accumulates at sharp corners of the nanoparticles leading to higher electron density at sharp edges/corner/tips of the nanoparticles, thus making the edged nanoparticles more reactive towards the bacterial cells (Goyal et al. 2017). The enhanced activity has also been attributed to interfacial atomic arrangements in the crystallographic facets of anisotropic AgNPs exposed to the environment (Goyal et al. 2017). Moreover, the anisotropic AgNPs are reported to be less toxic towards plants and other organisms in the environment as compared to spherical AgNPs (Goyal et al. 2017).

The photochemical method has been widely explored for synthesis of anisotropic AgNPs, such as nanorods, nanoprisms, nanodiscs, bipyramids, and decahedrons (Lee et al. 2013; Keunen et al. 2014; Saade and De Araújo 2014; Mukherji et al. 2018). The synthesis of anisotropic nanomaterials involves strong control on various reaction parameters. Controlled growth is required in specific dimensions to grow anisotropic structures from metallic silver (Jose et al. 2016). In the photochemical method, it is easy to control the reaction parameters and/or stop the reaction immediately by switching off the irradiation source to obtain AgNPs of the desired size and shape (Stamplecoskie and Scaiano 2010). Various surfactants, such as polyvinyl pyrrolidone (PVP), polyols, citrate, or ascorbic acid, have also been reported to direct the synthesis of anisotropic nanomaterials (Pietrobon et al. 2009; Jose et al. 2016). These surfactants preferentially bind to specific crystal faces of the nanoparticles, directing growth along a specific dimension. Researchers have demonstrated that photochemical methods employing appropriate stabilizing agents, such as PVP, may promote conversion of spherical AgNPs to anisotropic AgNPs (Pietrobon and Kitaev 2008; Chang et al. 2011; Jose et al. 2016; Li et al. 2016).

The antimicrobial properties strongly depend on the size and associated properties of AgNPs (Bae et al. 2010). Initial studies on antimicrobial and cytotoxic effects of AgNPs hypothesized that AgNPs primarily served as a source of Ag^+ ions; however, subsequent studies have demonstrated the direct effect of AgNPs which is significantly affected by their physicochemical properties, such as size, shape, and surface chemistry

(Pal et al. 2007; Bae et al. 2010; Agnihotri et al. 2014). Although numerous studies have demonstrated the antibacterial activity of anisotropic AgNPs, such as cubes, rods, wires, platelets, nanodiscs, and truncated triangular plates (Pal et al. 2007; Zhang et al. 2015; Helmlinger et al. 2016), no studies have explored the antimicrobial activity of decahedral silver nanoparticles. The focus of this study was to explore the antibacterial efficacy of decahedral AgNPs on selected strains of bacteria. The antibacterial activity of decahedral AgNPs was compared to the activity of spherical AgNPs of comparable size, so as to illustrate the effect of shape in determining the antibacterial efficacy. The decahedral AgNPs were synthesized using a photochemical approach, whereas the spherical AgNPs of comparable size were prepared by chemical reduction method. The antibacterial efficacy was tested against two Gram-negative and two Gram-positive bacterial strains commonly used for testing the antibacterial activity of antimicrobial agents. Alteration in shape may affect the dissolution behavior of AgNPs and/or their agglomeration behavior which in turn may affect their antimicrobial efficacy as opposed to the direct action of AgNPs (Bae et al. 2010). The dissolution pattern and agglomeration behavior of AgNPs are also expected to play a crucial role on the antibacterial effect of AgNPs, since the shape of AgNPs would affect the number of atoms on the surface. Hence, the dissolution behavior of both decahedral and spherical AgNPs was also studied to illustrate the mechanism controlling the antibacterial activity.

Materials and methods

Materials and reagents

Silver nitrate ($AgNO_3$), trisodium citrate (TSC), sodium borohydride ($NaBH_4$), and L-arginine were purchased from Merck (India). Polyvinylpyrrolidone (PVP, MW = 40 K) was obtained from Sigma Aldrich (USA). Other reagents, such as nitric acid and sulfuric acid, were obtained from Merck (Germany). *Escherichia coli* MTCC 443 and *Bacillus subtilis* MTCC 441 were procured from IMTECH, Chandigarh, and *Staphylococcus aureus* NCIM 5021 was procured from NCIM, Pune. *Pseudomonas aeruginosa* RS1 (GeneBank accession no. KF751345, MTCC 25391) was previously isolated from oily sludge (Dasgupta et al. 2018). Nutrient broth and bacteriological nutrient agar (both in powder form) were purchased from Himedia, Mumbai (India). All the analytical-grade reagents were used as received.

Photochemical synthesis of decahedral silver nanoparticles

Synthesis of decahedral AgNPs was done using the photochemical method, as described by Pietrobon and Kitaev (2008). Briefly, the seed solution was prepared by adding TSC (1 ml of 0.05 M), PVP (0.06 ml of 0.025 M), L-arginine (0.1 ml of 0.005 M), and $AgNO_3$ (0.4 ml of 0.005 M) into 14 ml of deionized water under stirred condition. Subsequently, the reduction of Ag^+ ions was initiated by adding 0.16 ml of 0.1 M $NaBH_4$ and stirring was continued for several minutes. The mixture immediately turned yellow indicating the formation of spherical AgNP seeds. Subsequently, synthesis of decahedral AgNPs was facilitated by exposing the yellow-colored seed precursor solution to blue LED light ($\lambda_{max} \approx 470$ nm) for 9 h. Finally, the nanoparticles were washed by centrifugation at 12,000 rpm for 30 min. The pellet was resuspended in water and stored in a refrigerator for further use.

Chemical synthesis of spherical silver nanoparticles

A two-step chemical reduction method was employed for synthesis of spherical AgNPs using the method reported by Agnihotri et al. (2014). Silver nitrate, sodium borohydride, and trisodium citrate were used as the metal precursor salt, reducing agent, and stabilizing agent, respectively, for synthesis of spherical AgNPs. The molar ratio of [$AgNO_3$]:[$NaBH_4$]:[TSC] was maintained as 1.22:0.5:2. To initiate AgNP synthesis, a mixture of $NaBH_4$ and TSC was prepared and mixed under vigorous stirring for 15 min at 60 °C. The $AgNO_3$ solution was added dropwise into the mixture to initiate synthesis of AgNPs under stirred condition. Subsequently, the completion of AgNP synthesis was accomplished by raising the solution temperature to 90 °C and stirring was continued until a stable wine-red color persisted. Finally, the colloidal solution of AgNPs was washed by centrifugation at 12,000 rpm for 30 min to get rid of unused chemicals and the nanoparticles were resuspended in deionized water. The colloidal AgNP solution was stored in a refrigerator at 4 °C until further use.

Characterization of silver nanoparticles

UV–vis absorbance spectra of the AgNPs were recorded using a UV–visible spectrophotometer (Schimadzu UV 1800, Japan) over the wavelength range of 800–200 nm at a resolution of 1 nm. The size and morphology of the AgNPs were characterized using field emission gun-transmission electron microscopy (FEG-TEM, JEOL, JEM-2100F, Japan) and field emission gun-scanning electron microscopy (FEG-SEM, JEOL-JSM 7600F, Japan). The sample for FEG-TEM analysis was prepared by mounting 10 μl of the diluted AgNP suspension on a copper grid followed by drying at room temperature. AgNP-loaded copper grids were also kept under an IR lamp to ensure complete dryness before observing them under FEG-TEM. The average size of AgNPs and their size distribution were analyzed by preparing a histogram considering more than 150 nanoparticles from multiple TEM micrographs using a Java image tool software, i.e., *Image J* software. Semi-quantitative elemental analysis of colloidal AgNPs was done using energy-dispersive X-ray spectroscopy (EDS) attached to an FEG-SEM instrument. The size distribution and stability of the AgNPs were determined using dynamic light scattering (DLS) and Zeta sizer (Zeta Pals, Brookhaven, USA) by measuring the zeta potential of the nanoparticle suspension. The yield of AgNPs was determined using the ratio of the mass of silver recovered after synthesis to the mass of silver added during synthesis. The concentration of synthesized decahedral AgNPs was determined by measuring the silver concentration in acid-digested AgNP solution using ICP-AES (ARCOS, SPECTRO Analytical Instruments, Germany).

Preparation of culture suspension of bacteria for inactivation studies

The nutrient broth (NB) media contained 1.3% of the nutrient broth powder in distilled water. For preparing nutrient agar (NA) plates, 2% nutrient agar was added to the NB, and the solution was autoclaved and cooled to 65 °C before pouring the plates. The NA layer applied on the plates was allowed to solidify at room temperature. NB media was used for growth and maintenance of the selected bacterial strains. A culture suspension of the selected bacterial strain was prepared for disinfection studies by growing them in the NB media. For preparing the inoculum for initiating a batch culture, each pure culture was grown up to end of log phase by incubating in a shaking incubator maintained at 180 rpm and a temperature of 37 °C. The grown culture was harvested by centrifugation at 10,000 rpm for 10 min and washed thrice using sterile phosphate buffer (pH 7.2). The washed culture was finally resuspended in phosphate buffer. The bacterial suspension was diluted with phosphate buffer so as to get unit absorbance at 600 nm. The bacterial concentration was quantified using the standard plate count technique. Unit absorbance of the bacterial suspension corresponded to ~ 10^8 CFU/ml. The stock culture was appropriately diluted to obtain a bacterial concentration of 10^3 CFU/ml for testing the antibacterial efficacy of the AgNPs. Finally, the culture stock was diluted to obtain a bacterial concentration of 10^3 CFU/ml for testing the antibacterial efficacy of the AgNPs. For antimicrobial activity studies, two Gram-positive bacteria, i.e., *Bacillus subtilis* MTCC 441 and *Staphylococcus aureus* NCIM 5021, and two Gram-negative bacteria, i.e., *Pseudomonas aeruginosa* RS1 and *Escherichia coli* MTCC 443, were used.

Determination of MIC and MBC of AgNPs

The antibacterial effect of the silver nanoparticles was tested using the four bacterial strains, and antibacterial efficacy was expressed in terms of minimum inhibitory concentration (MIC) and minimum bactericidal concentration (MBC). The MIC was determined by broth dilution method by conducting batch growth of specific cultures containing varying concentrations of decahedral AgNPs in suspension (2–10 μg/ml) using the procedure reported by Ruparelia et al. (2008). The study was performed in sterile Erlenmeyer flasks containing 100 ml nutrient broth containing 10^3 CFU/ml of the desired bacterial strain in the presence of varying concentrations of AgNPs. One positive control and one negative control were also used in this study. The uninoculated positive control contained NB with AgNPs. The inoculated NB media without AgNPs comprised the negative control. The cultures were incubated in an orbital shaker operating at 200 rpm and at 37 °C. High rotational speed was maintained to keep the nanoparticles in suspension throughout the duration of the experiment. At lower rpm, the nanoparticles may aggregate

and settle over time, thereby causing underestimation of antimicrobial activity. The absorbance at 600 nm was measured using a visible double beam spectrophotometer (Systronics Vis double Beam Spectro 1203, India) to depict bacterial growth in the flasks. The concentration, at which no increase in absorbance was observed, was reported as the MIC. The negative control exhibited normal growth in the absence of AgNPs. Similar experiments were conducted to determine the antibacterial activity of spherical AgNPs of comparable size. Studies were conducted over the AgNP concentration range 2–100 μg/ml. All the experiments were carried out in duplicate.

MBC was also determined by conducting batch culture studies followed by observing the presence or absence of bacterial growth on agar plates. For AgNP concentration beyond the MIC, a 50-μl sample from each flask was inoculated in nutrient agar plates by spread plate technique and the Petri plates were incubated at 37 °C for 24 h to allow microbial growth. The lowest concentration of AgNPs at which no viable colony was observed on the solid media was reported as the MBC (Ruparelia et al. 2008).

Dissolution of silver nanoparticles

To understand the behavior of AgNPs in different aqueous environments and their impact on antibacterial efficacy, dissolution studies were conducted using decahedral and spherical AgNPs in water as well as nutrient broth. Silver nanoparticles (final concentration after dissolution, 10 μg/ml) were dissolved in distilled water and nutrient broth and were kept under shaking condition. The absorption spectra and hydrodynamic size of AgNPs were measured for 5 h in nutrient broth and distilled water under shaking condition. To determine the role of silver ions in antibacterial activity, the nanoparticles suspended in water and nutrient broth were ultracentrifuged at 25,000 rpm for 2 h and the concentration of silver was determined in the supernatant using ICP-AES. The pelleted nanoparticles were resuspended in water, and their mean hydrodynamic diameter was determined using dynamic light scattering (DLS, Zeta Pals, Brookhaven, USA). The change in morphology of the nanoparticles as a result of dissolution and/or aggregation was determined by imaging the nanoparticles in FEG-TEM.

Results and discussion

Synthesis of decahedral silver nanoparticles

Synthesis of decahedral AgNPs was done using photochemical methods which requires multiple growth/regrowth steps to produce the decahedral AgNPs of controlled shape and size. The photochemical synthesis route requires small quasi-spherical AgNP seeds, referred to as plasmonic seeds that can be synthesized through chemical reduction of a silver salt using $NaBH_4$. These seeds undergo shape transformation by reducing the activation energy under visible light irradiation (Xie et al. 2016). In this study, the synthesis of decahedral AgNPs was achieved through photochemical transformation of spherical AgNP seeds to decahedral AgNPs upon irradiation using LED light of wavelength 470 nm. The synthesis was initiated with the reduction of silver ions by sodium borohydride to generate the primary seed precursor of AgNPs. The formation of seed AgNPs was revealed by the appearance of a yellow color in the seed precursor solution. UV–vis spectra provided confirmation by exhibiting the localized surface plasmon resonance (LSPR) peak at 405 nm (shown in Fig. A1, ESI). Addition of TSC and PVP contributed towards improving the colloidal stability of the AgNPs through electrostatic and steric stabilization, respectively. Visible light may have also caused the reduction of silver ions to AgNPs in the presence of TSC and seed AgNPs. It is reported that stabilization of AgNPs is achieved through electrostatic repulsion caused by the free carboxylic acid group of TSC on the AgNPs. The other two carboxylic acid groups of TSC attach and facilitate electron transfer on the surface of the nanoparticles owing to their nucleophilic nature leading to further reduction of Ag^+ ions (Maillard et al. 2003). Subsequently, L-arginine was added to the yellow-colored seed precursor solution and was exposed to irradiation using blue LED ($\lambda_{max} \approx 470$ nm) for 9 h to facilitate the synthesis of decahedral AgNPs. L-Arginine is reported to control the size and shape during the synthesis of decahedral AgNPs (Pietrobon and Kitaev 2008; Mukherji et al. 2018). During irradiation, L-arginine played a vital role in maintaining uniform growth of the decahedral AgNPs. Arginine may have formed a complex with the citrate-coated negatively charged AgNPs thereby reducing their negative charge and enhancing their reactivity (Murshid 2013). The regrowth of seed AgNPs may have occurred upon irradiation as

the localized surface plasmon resonance peak of decahedral AgNPs matched with the wavelength maxima of the LED light. This phenomenon facilitated the synthesis of monodispersed decahedral AgNPs by minimizing the generation of silver nanoprisms and nanoplates in solution (Mukherji et al. 2018). Thus, L-arginine acted as a photochemical promoter which slowed down the growth of larger silver platelets/prisms in the AgNP precursor solution through relatively strong binding to the AgNP platelets and favored the growth of decahedral AgNPs (Pietrobon and Kitaev 2008b; Zheng et al. 2009a). The completion of decahedral AgNP synthesis was accompanied by color change of the solution from light yellow to brown with a greenish shine. The chemical reduction method was employed for synthesis of spherical AgNPs, as reported by Agnihotri et al. (2014). The synthesized nanoparticles were washed by centrifugation; the pellets were resuspended in DI water and subsequently used for characterization and antibacterial studies.

Characterization of decahedral and spherical silver nanoparticles

The change in color of the seed solution from yellow to brown with greenish tinge revealed the synthesis of decahedral AgNPs. A single sharp peak at 502 nm was observed in the UV–vis spectra, as shown in Fig. 1. The peak was due to the LSPR of the decahedral AgNPs with average size 52 nm and side length of 33 nm. A very small peak was also observed at around 405 nm, as in the yellow-colored seed precursor of AgNPs. This possibly corresponded to the presence of a few spherical silver nanoparticles in the colloidal suspension of decahedral AgNPs.

The best shape selectivity and size distribution of decahedral AgNPs could be achieved by optimizing the PVP concentration. Lower PVP concentration or absence of PVP may lead to reduced stability of decahedral AgNPs, which may subsequently result in the generation of aggregated ill-defined large AgNPs. Although the key role of PVP is that of a steric stabilizer, it also improved the stability and monodispersivity of the nanoparticles. However, higher concentrations of PVP (> 0.8 mM) may cause increased polydispersity of the decahedral AgNPs and may also promote the synthesis of distorted decahedral particles. The role of intense blue light irradiation and constant plasmonic excitation is analogous to oxidative etching as reported in the polyol process and use of peroxide in thermal approaches for preparation of silver prisms (Pietrobon and Kitaev 2008). The spherical seed AgNPs were inherently unstable under continuous excitation. Upon light irradiation, two processes, i.e., growth of platelets and growth of decahedra, occurred simultaneously. During exposure to light, the AgNPs in solution remained in a state of dynamic equilibrium, where the size of the final nanoparticles was dependent on the wavelength and intensity of incident light. However, the final shape of the nanoparticle depends on the morphologies present in the seed precursor solution and their relative stability. The platelets were relatively less stable as compared to the decahedral nanoparticles. Hence, they were dissolved in the solution and the silver released was incorporated into the growing decahedral seeds upon further irradiation. Thus, decahedral nanoparticles were obtained as the exclusive final product. Only the decahedral AgNPs remained in the solution upon irradiation, as also illustrated by Pietrobon and Kitaev (2008). A uniform decahedral shape of the synthesized AgNPs was revealed through FEG-TEM and FEG–SEM images (Fig. 2). The diameter of decahedral AgNPs was determined as 52.1 ± 5.7 nm from FEG-TEM image analysis, and their side length was 33.2 ± 3.1 nm. The formation of decahedral AgNPs may be attributed to PVP, a shape-directing stabilizer, which preferentially binds to silver {100} facets and promotes the growth of seed nanoparticles into tetrahedral and subsequently into decahedral nanoparticles. An interatomic distance of ~ 2.35 Å demonstrated that each decahedral AgNP was bound by {111} facets, as revealed through the TEM images (Fig. S2, ESI) (Rojas-Andrade et al. 2015; Zheng et al. 2009).

Spherical AgNPs of average size 50 nm were synthesized using the chemical reduction approach reported by Agnihotri et al. (2014). The presence of an LSPR peak at 416 nm revealed the synthesis of spherical AgNPs (Fig. 3). A uniform spherical shape of the synthesized AgNPs was also revealed by FEG-TEM images (Fig. 3b). The average size of spherical AgNPs from FEG-TEM image analysis was determined as 44.2 ± 6.3 nm with a size range of 28–61 nm.

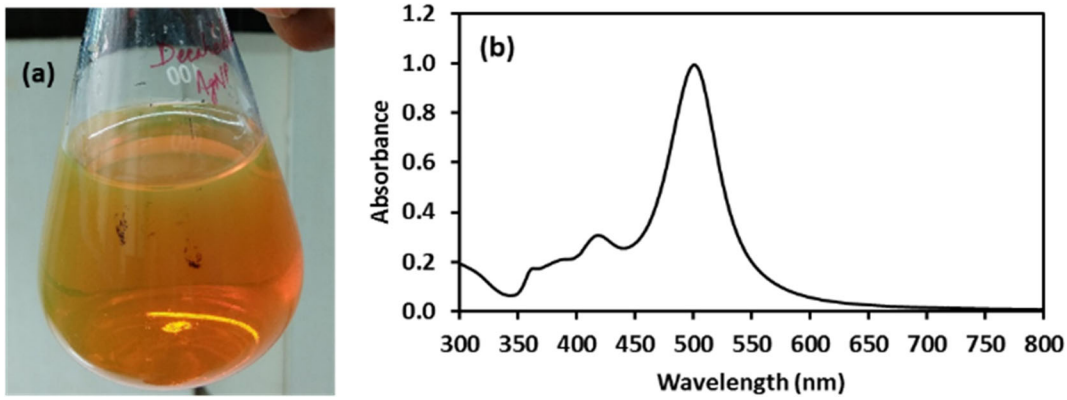

Fig. 1 **a** Decahedral AgNPs, **b** UV–vis spectra of AgNPs

Shape-controlled antibacterial activity of silver nanoparticles

Antibacterial activity of decahedral silver nanoparticles

The effect of varying concentrations of decahedral AgNPs was tested against two Gram-negative bacteria, i.e., *E. coli* MTCC 443 and *P. aeruginosa* RS1, and two Gram-positive strains, i.e., *B. subtilis* MTCC 441 and *S. aureus* NCIM 5021. Representative growth profiles of selected strains in the presence of decahedral AgNPs for the concentration range of 2–10 μg/ml are shown in Fig. 4. The MIC values determined based on growth curves at varying concentrations of the decahedral silver nanoparticles (Fig. 4) and MBC values for all the selected bacterial strains are shown in Table 1. No variation in MIC and MBC due to decahedral silver nanoparticles was observed for the duplicate experiments for any of the bacterial strains tested. The MIC value was 4 μg/ml for *B. subtilis* MTCC 441, 6 μg/ml for *E. coli* MTCC 443 and *P. aeruginosa* RS1, and 8 μg/ml for *S. aureus* NCIM 5021. The corresponding MBC values

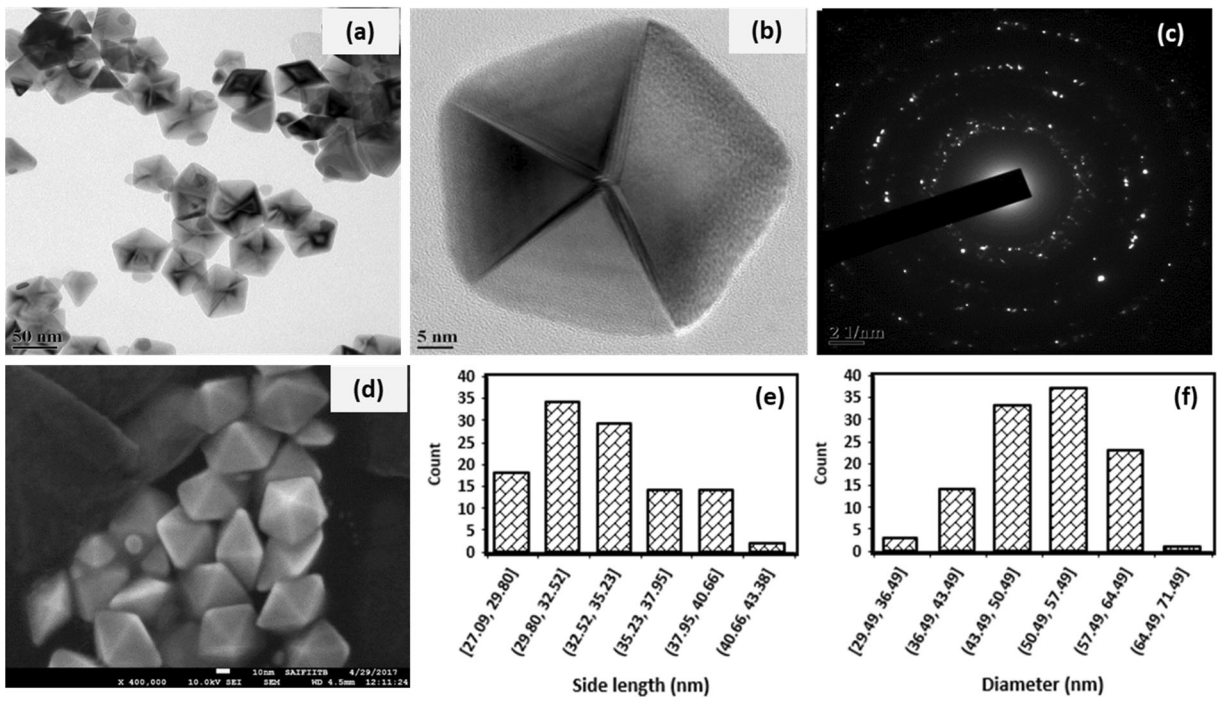

Fig. 2 **a**, **b** FEG-TEM images, **c** selected area electron diffraction (SAED) ring pattern, **d** FEG-SEM images, and **e**, **f** histogram depicting the distribution of side length and diameter of decahedral AgNPs, respectively

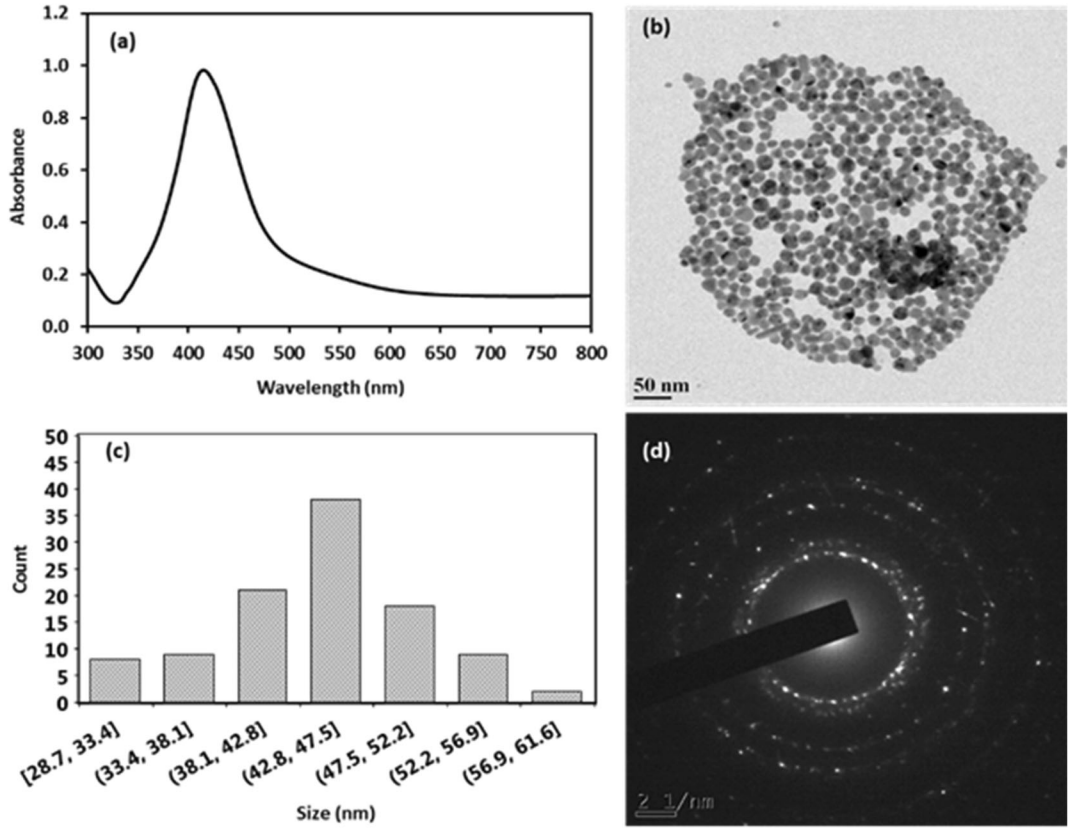

Fig. 3 **a** UV–vis spectra, **b** FEG-TEM images, **c** histogram depicting the size distribution, and **d** SAED pattern of spherical AgNPs

were 6 μg/ml for *E. coli* MTCC 443, 8 μg/ml for *P. aeruginosa* RS1 and *B. subtilis* MTCC 441, and 10 μg/ml for *S. aureus* NCIM 5021. Thus, in terms of bactericidal effect, *E. coli* MTCC 443 was found as the most sensitive strain (lowest MBC among all strains), while in terms of growth inhibition, *B. subtilis* was the most sensitive strain (lowest MIC among all strains). *S. aureus* NCIM 5021 was observed to be the most resistant among the four selected bacterial strains (highest MIC and MBC). Usually, Gram-negative bacteria are reported to be more sensitive to antimicrobials than Gram-positive bacteria; however, a higher sensitivity of *B. subtilis* was found for decahedral AgNPs in this study. Some researchers have also reported relatively higher sensitivity of *B. subtilis* to silver and copper nanoparticles compared to *E. coli* and *S. aureus* (Yoon et al. 2007; Ruparelia et al. 2008; Li et al. 2013; Dasgupta et al. 2015). In general, for most antimicrobials, bacteriostatic action (measured using MIC) is observed at a slightly lower concentration of the antimicrobial agent than bactericidal action (measured using MBC). However, in the literature, a few studies have reported identical MIC and MBC values for specific strains, while some others have shown MBC that is 4–5 times higher than the MIC for specific strains (Ruparelia et al. 2008; Valodkar et al. 2011; Pencheva et al. 2012; Vellora et al. 2013; Dasgupta et al. 2015) (Table S2, ESI). Thus, when comparing across various strains, the trends in variation of MIC and MBC may differ as seen in this study for the decahedral nanoparticles (Table 1). The effectiveness of antimicrobial agents is determined by various factors, including the nature of the antimicrobial agent, the target pathogen, and the interaction of the antimicrobials with the target site of the pathogen (Li et al. 2017).

From Fig. 4a, it was also observed that with increasing concentration of decahedral AgNPs below the MIC, *E. coli* shows an increase in the lag phase and a decrease in maximum absorbance at the end of the log phase. *P. aeruginosa* showed an increased lag phase in the presence of the decahedral AgNPs below the MIC; however, the maximum absorbance was almost comparable to that of the negative controls (Fig. 4b). Decahedral AgNPs at 2 μg/ml had no inhibitory effect

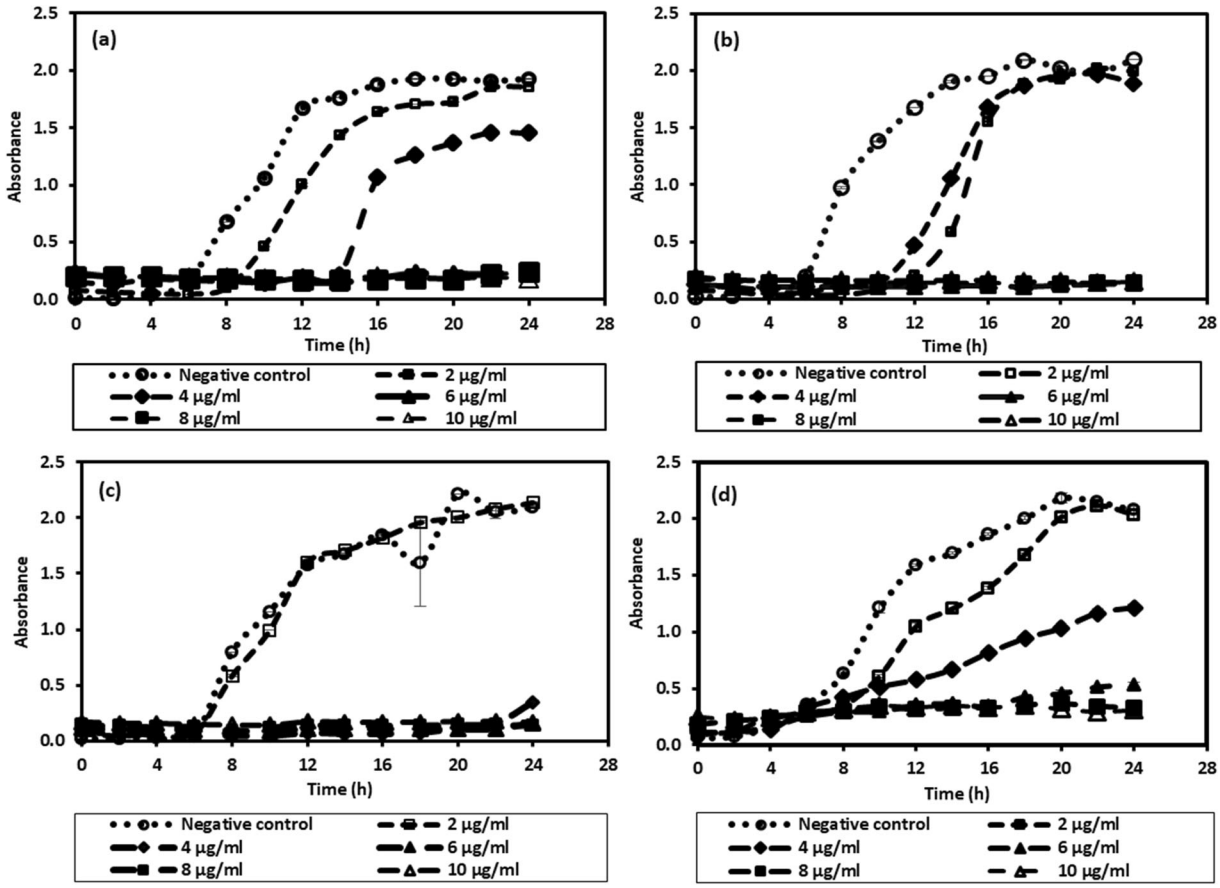

Fig. 4 Representative growth profile in the presence of varying concentrations of decahedral AgNPs for bacterial strains **a** *E. coli*, **b** *P. aeruginosa*, **c** *B. subtilis*, and **d** *S. aureus*

on culture growth in *B. subtilis* while 4 µg/ml completely inhibited culture growth (Fig. 4c). In *S. aureus*, the growth rate and the maximum absorbance progressively decreased as the concentration of decahedral AgNPs increased from 2 to 6 µg/ml, until growth ceased completely at 8 µg/ml.

Along with the characteristics of nanoparticles, i.e., size, shape, crystallinity, and surface properties of nanoparticles, significant variation in antimicrobial activity may result due to difference in initial concentration, nutrient media, and the strains used. Both Agnihotri et al. (2014) and Ruparelia et al. (2008) have reported the MIC of spherical AgNPs on several of the bacterial strains that are used in this study; however, the average size of AgNPs used was much smaller. Hence, antibacterial studies were also

Table 1 MIC and MBC values of decahedral AgNPs for the selected bacterial strains

Culture	Decahedral AgNPs		Spherical AgNPs	
	MIC (µg/ml)	MBC (µg/ml)	MIC (µg/ml)	MBC (µg/ml)
E. coli MTCC 443	6	6	40	60
P. aeruginosa RS1	6	8	60	80
B. subtilis MTCC 441	4	8	60	80
S. aureus NCIM 5021	8	10	80	100

MIC minimum inhibitory concentration, *MBC* minimum bactericidal concentration

conducted using spherical AgNPs of comparable size under similar experimental conditions, i.e., using the same media and the same initial bacterial concentration as reported by Ruparelia et al. (2008).

Antibacterial activity of spherical silver nanoparticles

Spherical AgNPs of similar size range, as the decahedral AgNPs, exhibited MIC in the range of 40–80 μg/ml and MBC in the range of 60–100 μg/ml (Fig. 5). The results are summarized in Table 1. No variation in MIC and MBC values was found due to both spherical and decahedral silver nanoparticles for the duplicate experiments for any of the bacterial strains. The MIC values were 40 μg/ml for *E. coli* MTCC 443, 60 μg/ml for *B. subtilis* and *P. aeruginosa*, and 80 μg/ml for *S. aureus*. The corresponding MBC values were 60 μg/ml for *E. coli* MTCC 443, 80 μg/ml for *P. aeruginosa* RS1 and *B. subtilis* MTCC 441, and 100 μg/ml for *S. aureus* NCIM 5021. In terms of growth inhibition and bactericidal effect, *E. coli* MTCC 443 was found to be the most sensitive strain whereas *S. aureus* NCIM 5021 was observed to be the most resistant among the four bacterial strains tested. The presence of spherical AgNPs at a concentration below the MIC increased the lag phase and decreased the maximum absorbance in *E. coli*, while in *P. aeruginosa*, *B. subtilis*, and *S. aureus*, a decreased growth rate and lower maximum absorbance were observed (Fig. 5a–d).

This study revealed significantly higher antibacterial efficacy of decahedral AgNPs as compared to spherical AgNPs of comparable size and also as compared to spherical AgNPs of lower size. In a study by Agnihotri et al. (2014), MIC values of chemically synthesized AgNPs of comparable size (~ 50 nm) were reported to be much higher for all the strains, i.e., 80, 100, and 160 μg/ml for *E. coli* MTCC 443, *B. subtilis*, and *S. aureus*, respectively; however, they conducted the studies at a higher initial concentration of bacteria, i.e., 10^4–10^5 CFU/ml (Agnihotri et al. 2014). In another study by Ruparelia et al. (2008), strain-specific sensitivity of silver nanoparticles (average size, 3.3 nm) was demonstrated through batch mode antimicrobial studies with an initial bacterial concentration of 10^3–10^4 CFU/ml in nutrient broth. Among various tested bacterial strains, *E. coli* MTCC 443 was found to be most sensitive to spherical AgNPs and its MIC was 40 μg/ml. In contrast, another strain of *E. coli*, i.e., MTCC 739, was more resistant and exhibited an MIC of 180 μg/ml. *B. subtilis* MTCC 441 had an MIC comparable to that of *E. coli* MTCC 443 whereas various strains of *S. aureus* exhibited MIC values in the range of 120 to 140 μg/ml for these spherical AgNPs.

Thus, decahedral AgNPs exhibited much higher bactericidal efficacy towards all the selected bacterial strains. The MBC of decahedral AgNPs was consistently tenfold lower than that of spherical AgNPs of comparable size, and the trend observed across strains was consistent. The MIC was almost ten times lower; however, some variation in sensitivity was observed for spherical and decahedral AgNPs. On the basis of these studies, it can be concluded that edged silver nanoparticles, such as decahedral AgNPs can exhibit broad-spectrum bactericidal activity towards many different microbial strains in a more effective manner as compared to spherical silver nanoparticles as also reported in the literature (Rojas-Andrade et al. 2015; Goyal et al. 2017).

Behavior of AgNPs dispersed in distilled water and nutrient broth

To understand the behavior of AgNPs in different aqueous environments and their impact on antibacterial efficacy, absorption spectra and hydrodynamic size of AgNPs were measured for 5 h in nutrient broth and distilled water under shaking condition at 200 rpm in a rotary shaker. To determine the role of silver ions on antibacterial activity, dissolution studies were separately conducted for decahedral and spherical AgNPs in water and nutrient broth. The absorption spectra showed only minor changes over time when decahedral and spherical AgNPs were dispersed in water, however, a significant decrease in absorbance was observed when decahedral and spherical AgNPs were dispersed in NB media (Fig. 6). A significant decrease in absorbance was observed over the first 3 h for both decahedral as well as spherical AgNPs dispersed in NB, while only a slight decrease was observed between 3 and 5 h (Fig. 6). There was no change in absorbance spectra beyond 5 h. For the spherical AgNPs dispersed in NB, in addition to a decrease in absorbance, a broad absorbance spectrum was seen in the wavelength range of 400–600 nm. This may be attributed to aggregation of AgNPs and their transformation into larger-sized nanoparticles. FEG-TEM imaging of the spherical and decahedral AgNPs dissolved in NB for 5 h also confirmed the aggregation of AgNPs (Fig. 7). Aggregation of AgNPs was higher in

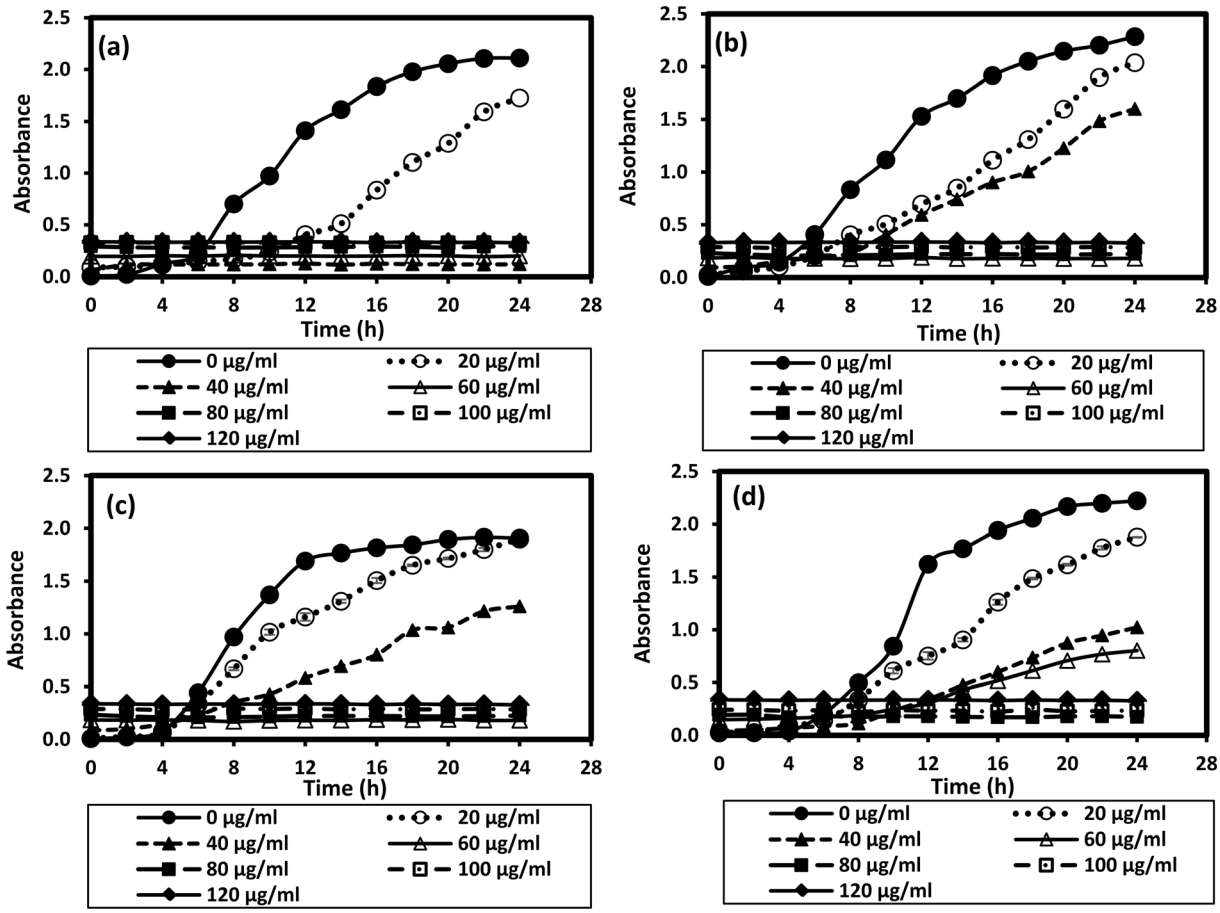

Fig. 5 Representative growth profile in the presence of varying concentrations of spherical AgNPs for bacterial strains **a** *E. coli*, **b** *P. aeruginosa*, **c** *B. subtilis*, and **d** *S. aureus*

the case of spherical AgNPs as compared to decahedral AgNPs. FEG-TEM images also revealed a significant aggregation in the case of spherical AgNPs dispersed in NB, whereas decahedral AgNPs exhibited a lower extent of aggregation (Fig. 7). In addition, FEG-TEM images also revealed a wide variation in size as a result of aggregation in both the cases (Fig. 7).

These results were also supported by DLS. The hydrodynamic diameter of decahedral and spherical AgNPs dispersed in NB media increased from 78 to 266 nm and from 104 to 444 nm, respectively, over 5 h. In contrast, the hydrodynamic diameter of decahedral and spherical AgNPs in deionized water showed only a slight decrease from 77 to 74 nm and from 69 to 58 nm, respectively, over 5 h. The change in the hydrodynamic diameter of decahedral and spherical AgNPs in NB media confirmed the agglomeration of nanoparticles over time. However, the slight decrease in hydrodynamic diameter of decahedral and spherical AgNPs observed in DI water may be attributed to the dissolution of AgNPs to form Ag^+ ions. These results are consistent with those reported by Roh et al. (2013). The observations may be explained by the fact that the spherical AgNPs were stabilized by citrate ions whereas decahedral AgNPs were stabilized by PVP. Citrate contains three carboxyl groups ($–COO^-$), such that the surface of citrate-coated AgNPs carries a higher negative charge. Thus, the citrate-coated AgNPs are primarily stabilized by electrostatic repulsion which reduces their aggregation in colloidal suspension. However, PVP contains a pyrrolidone group, a cyclic organic structure having carbon and oxygen double bonds. The coating of pyrrolidone groups on the surface of decahedral AgNPs is expected to cause stabilization through steric repulsion (Roh et al. 2013). The presence of carbon and oxygen double bonds in the pyrrolidone group may also induce a weak negative surface charge on the PVP-coated AgNPs (Roh et al. 2013). Thus, the

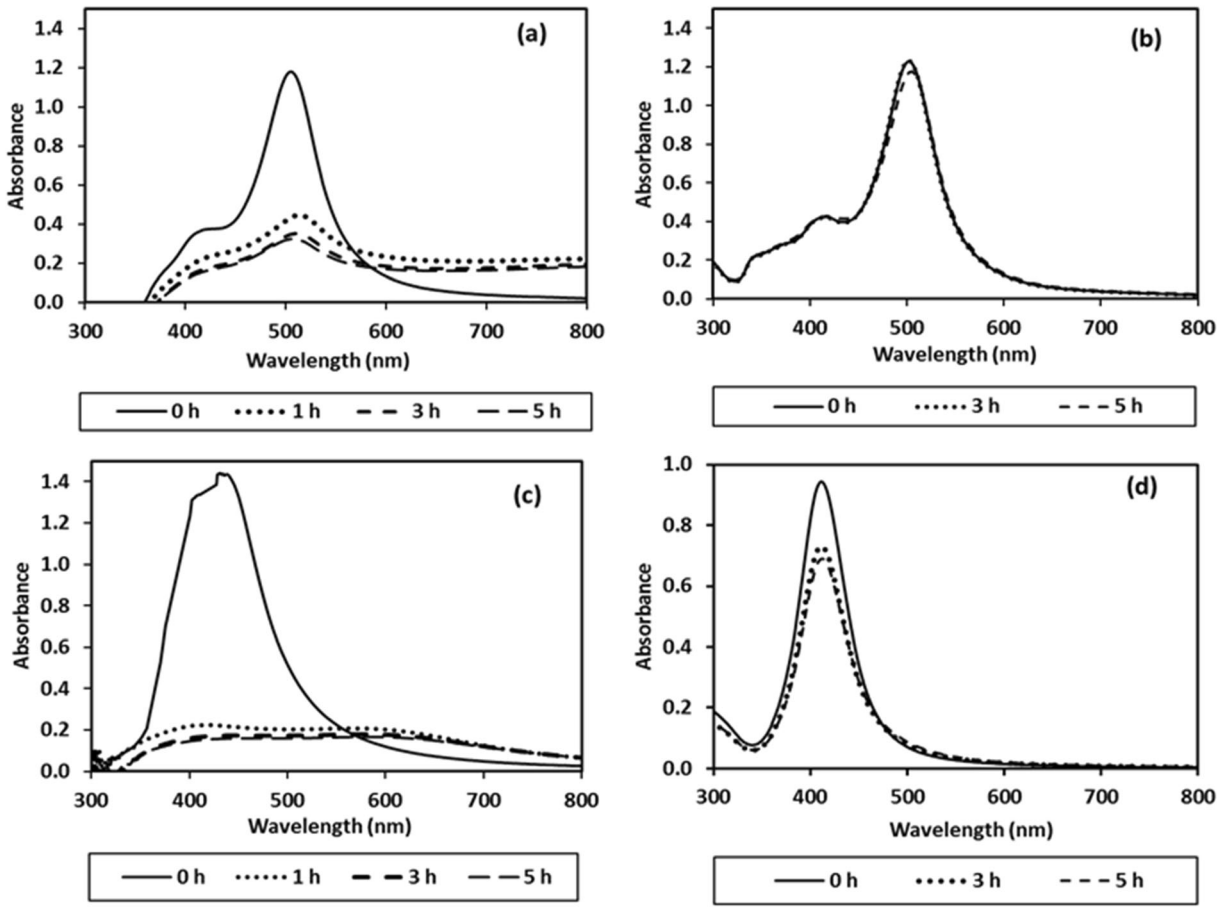

Fig. 6 UV–vis spectra depicting change in the LSPR peak on dissolution of **a**, **b** decahedral AgNPs and **c**, **d** spherical AgNPs in NB (**a**, **c**) and water (**b**, **d**)

stability of a dispersion of PVP-coated decahedral AgNPs may be attributed to the combined effect of steric hindrance and electrostatic repulsion.

The complex nature of nutrient broth consisting of several salts, such as NaCl, and protein components may have promoted flocculation among adjacent AgNPs (Roh et al. 2013). Protein and other biological components of nutrient broth may have interacted with the surface of AgNPs, thereby leading to formation of protein corona, which largely defines the biological identity of the nanoparticles (Roh et al. 2013; Shannahan et al. 2013). Due to this effect, the size of the AgNPs may have increased when dispersed in NB. The protein corona may have lowered the surface charge and reduced the electrostatic repulsion without showing any effect on steric repulsion (Casals et al. 2010; Roh et al. 2013). This may explain why the citrate-coated spherical AgNPs exhibited higher extent of aggregation as compared to the PVP-coated decahedral AgNPs, where steric repulsion also contributed to stabilization of the AgNPs. This result was also consistent with those reported by Roh et al. (2013). Thus, the PVP-coated AgNPs, stabilized by steric as well as electrostatic repulsion, exhibited better dispersion stability in biological media, as compared to the citrate-coated AgNPs, stabilized only by electrostatic repulsion.

To further confirm the dissolution of decahedral and spherical AgNPs used in this study, the AgNP suspension (10 μg/ml in each case) after 5 h dissolution was centrifuged at 25,000 rpm for 1.5 h to separate out the nanoparticles from the aqueous phase. The supernatant was analyzed for silver content using ICP-AES. The aqueous phase concentrations of silver ions for the decahedral and spherical AgNPs dispersed in water were in the range of 64–152 μg/l and 22–25 μg/l, respectively, while the corresponding values for the decahedral and spherical AgNPs dispersed in NB media were in the range of 115–158 μg/l and 66–92 μg/l,

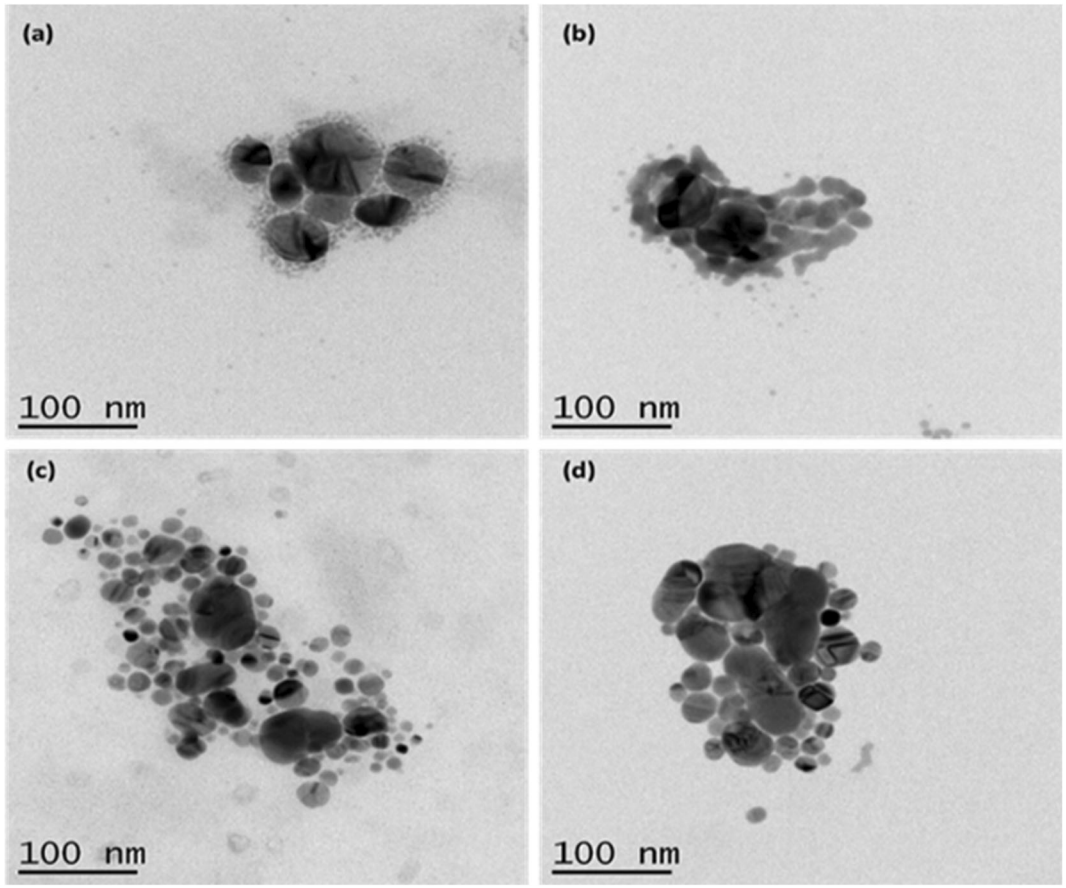

Fig. 7 FEG-TEM images of **a**, **b** decahedral AgNPs and **c**, **d** spherical AgNPs dispersed in **a**, **c** distilled water and **b**, **d** NB after a contact time of 5 h under shaking condition

respectively. Thus, it is evident from the dissolution studies that enhanced antibacterial activity of the decahedral AgNPs was not solely due to the slightly higher dissolution of AgNPs to Ag^+ ions. However, the slightly higher silver ion concentration observed for the decahedral AgNPs may also have partly contributed to the higher antibacterial effect. Both shape as well as surface charge of silver nanoparticles possibly played a crucial role in bacterial inactivation. Thus, the shape and surface charge of AgNPs may be exploited to further enhance the antibacterial effect of AgNPs.

Bacterial inactivation by the decahedral and spherical silver nanoparticles

The antimicrobial activity of AgNPs is dependent on various factors, including size, shape, surface charge, and capping/stabilizing agent (Pal et al. 2007; El Badawy et al. 2011; Agnihotri et al. 2014; Hong et al. 2016; Helmlinger et al. 2016). The antibacterial activity has been reported for anisotropic AgNPs having a distinct shape and morphology, such as cubes, rods, wires, platelets, nanodiscs, and truncated triangular plates (Pal et al. 2007; El Badawy et al. 2011; Zhang et al. 2015; Rojas-Andrade et al. 2015; Helmlinger et al. 2016; Goyal et al. 2017). However, no previous studies have explored the antibacterial activity of decahedral AgNPs. Pal et al. (2007) demonstrated that truncated triangular silver nanoplates exhibited stronger biocidal action on *E. coli* compared to rod-shaped and spherical AgNPs and Ag^+ ions. In another study, Hong et al. (2016) demonstrated that silver nanocubes exhibited higher antibacterial activity compared to nanospheres, while nanowires displayed the weakest antibacterial activity. However, some studies have also reported comparable antibacterial activity, irrespective of the shape of AgNPs (Helmlinger et al. 2016; Raza et al. 2016). Based on the zone inhibition test, Cheon et al. (2019) reported that the

antimicrobial activity decreased in the order spherical AgNPs > disk-shaped AgNPs > triangular plate AgNPs. The antimicrobial activity of the AgNPs was correlated with the surface area–dependent release rate of Ag^+ ions (Cheon et al. 2019). For antimicrobial activity based on the zone inhibition test, the diameter of the inhibition zone may depend on the solubility and infusibility of the test material, such that its full antibacterial potential may not be revealed. It is not possible to directly compare antibacterial activity across different studies since the results may be affected by factors such as the microbial strain used, the initial concentration of the microorganism, the media used and the characteristics of nanoparticles, methodologies adopted for testing their antibacterial efficacy, and the interaction of antimicrobials at the site of attachment to bacterial cell surfaces (Mukherji et al. 2012; Li et al. 2017). The composition of the media may also affect the physicochemical properties of nanoparticles which in turn may affect their dissolution behavior, interaction with bacteria, and bactericidal effect.

When comparing spherical AgNPs of varying size, the smaller AgNPs with a higher surface to volume ratio are more effective in their bactericidal action (Agnihotri et al. 2014). The higher efficacy of the smaller-sized AgNPs may be due to the fact that they directly penetrate into the cells and release silver ions into the periplasmic space. The AgNPs may directly bind to the intracellular biomolecules, causing disruption of essential biochemical processes, and eventually lead to inactivation/killing. Although the surface to volume ratio of spherical AgNPs is higher than for decahedral nanoparticles, the bactericidal efficacy of the spherical AgNPs is lower than for the decahedral AgNPs. It has been proposed that nanoparticles with sharp edges exhibit higher activity due to less activation energy requirement for edged/anisotropic nanoparticles. It has been demonstrated that the surface charge accumulates at sharp corners of the nanoparticles leading to higher electron density at sharp edges/corner/tips of the nanoparticles, thus making the edged nanoparticles more reactive towards the bacterial cells (Goyal et al. 2017). This is mainly due to the presence of a larger number of valence unsatisfied surface atoms at the edges and corners of the AgNPs. Moreover, the activity of faceted nanoparticles, such as decahedral nanoparticles, is enhanced by the atomic arrangements in the interfaces of the exposed crystal and the crystallographic facets exposed to the surrounding medium (Goyal et al. 2017; Murph et al. 2017; Rojas-Andrade et al. 2015). Facet engineering of nanomaterials has significant potential in biological applications (Qi et al. 2020). With AgNPs of varying shape, it has been demonstrated that the enhanced activity of the faceted nanostructures strongly depends on the surface morphologies. Triangular nanoprisms, nanotetrahedra, and nanodecahedra are faceted predominantly by highly reactive {111} surfaces. These nanostructures exhibit strong affinity to sulfur-containing membrane proteins and oxygen-containing functional groups on bacterial cell surfaces (Rojas-Andrade et al. 2015). The presence of such reactive facets in decahedral AgNPs possibly allows their efficient interaction with the bacterial cell surfaces causing physical disruption of the bacterial cell walls and cell membrane and free radical-induced peroxidation of membrane lipids. Subsequent changes in membrane permeability may adversely affect cellular respiration and inhibit metabolism in bacterial cells. With an increase in concentration of decahedral nanoparticles, these effects were revealed through the changes in growth rate and the duration of lag phase. The faceted AgNPs demonstrated a tenfold lower MIC and MBC in comparison to the spherical AgNPs. It has also been demonstrated that nanoparticles can interact with various biological components, including lipid, peptides, and proteins. Such interactions form a protein corona (PC) on their surface, which is dependent on various factors, such as physical and chemical properties of nanoparticles as well as biological media. The formation of a protein corona in the system may affect its bioavailability, efficacy, and cytotoxicity due to changes to its shape, size, surface charge, and interfacial characteristics (Shannahan et al. 2013). Apart from these factors dominated by the distinct shape and morphology of the decahedral silver nanoparticles, some additional factors may have affected the results. PVP used as stabilizer for the decahedral AgNPs may have influenced the antibacterial activity by lowering the surface charge of the decahedral nanoparticles and facilitating better interaction with the bacteria cells. The higher rate of release of Ag^+ ions from the decahedral AgNPs may have also partly enhanced their antibacterial activity.

The decahedral AgNPs depicted tenfold lower MIC and MBC values compared to spherical nanoparticles of comparable size across all the four bacteria tested. *E. coli* and *P. aeruginosa* are Gram-negative bacteria, while *B. subtilis* and *S. aureus* are Gram-positive bacteria. The outer lipopolysaccharide (LPS) layer of Gram-negative bacteria would initially interact with the antibacterial agent in Gram-negative bacteria. In Gram-positive bacteria, the peptidoglycan layer would initially

interact with the nanoparticles. Moreover, in some bacteria, extracellular polymeric substances (EPS) are present on the cell surfaces forming a slime layer or capsule. Both Gram-positive and Gram-negative bacteria are reported to carry a negative charge which varies with variation in solution pH (Chakraborty et al. 2010). The functional groups on the bacterial cell surface, i.e., carboxyl, phosphate, and amino groups, are responsible for their surface charge (Mohanty and Mukherji 2012). The negative charge on both bacterial cells and AgNPs would promote repulsion and thereby reduce the antibacterial action of AgNPs (El Badawy et al. 2011). Further studies with a wider range of bacterial strains can be designed to explore how the nature of the bacterial cell surface, bacterial cell surface charge, and EPS may affect their interaction with the decahedral and spherical AgNPs.

In this manuscript, the antibacterial efficacy of decahedral AgNPs on bacteria was explored for the first time and compared with that of spherical nanoparticles. Numerous studies have demonstrated the antibacterial activity of anisotropic AgNPs, such as cubes, rods, wires, platelets, nanodiscs, and truncated triangular plates (Pal et al. 2007; Zhang et al. 2015; Rojas-Andrade et al. 2015; Hong et al. 2016; Helmlinger et al. 2016); however, no prior studies have explored the antimicrobial activity of decahedral silver nanoparticles. It is well known that the antimicrobial activity of AgNPs is dependent on various factors, including size, shape, surface charge, and capping/stabilizing agent (Pal et al. 2007; El Badawy et al. 2011; Agnihotri et al. 2014; Helmlinger et al. 2016). However, although various studies have demonstrated the shape-dependent bacterial inactivation for anisotropic AgNPs (Pal et al. 2007; El Badawy et al. 2011; Rojas-Andrade et al. 2015; Goyal et al. 2017), comparing the effectiveness of other shapes to that of decahedral AgNPs was not feasible due to differences in the bacterial strains, growth media, and initial concentration used; differences in size of the AgNPs; and differences in antibacterial efficacy testing methodologies adopted across different studies. The growth media may affect the physicochemical properties of AgNPs, which, in turn, may affect their interaction and dissolution behavior and correspondingly impact their antibacterial efficacy. Moreover, although the main objective of this work was to reveal the impact of shape while keeping the nanoparticle size, bacterial strains, growth media, and initial number concentration constant, studies employing identical synthesis protocols and reagents are rare. The additional reagents used to achieve synthesis of stable decahedral AgNPs may have also partly influenced the antibacterial activity. This study also revealed the release of silver ion from both decahedral and spherical AgNPs. Silver ion release may eventually decrease the overall effectiveness of the AgNPs over time. Moreover, alteration in size of both the spherical and decahedral AgNPs may have occurred due to aggregation of the nanoparticles over time. Such aggregation is expected to decrease their antibacterial efficacy. This disadvantage of colloidal AgNPs may be avoided through immobilization of the AgNPs.

Conclusion

Decahedral silver nanoparticles were successfully synthesized using a photochemical approach. UV–vis spectra indicated synthesis of decahedral AgNPs by showing a peak at 502 nm. The size and shape of the synthesized nanoparticles were determined by microscopic imaging under FEG-SEM and FEG-TEM. Analysis of micrographs demonstrated the average diameter of decahedral silver nanoparticles as 52 nm and side length as ~ 33 nm. Spherical AgNPs synthesized using the chemical reduction approach exhibited an LSPR peak at 416 nm. FEG-TEM images revealed spherical shape of the AgNPs with average size 44.2 and size range of 28–61 nm. The decahedral AgNPs exhibited much higher bactericidal efficacy towards all the selected bacterial strains. Decahedral AgNPs exhibited MIC in the range of 4–8 μg/ml, which was almost tenfold lower than the MIC of spherical AgNPs of comparable size. The MBC of decahedral AgNPs (6–10 μg/ml) was also consistently tenfold lower than that of spherical AgNPs of comparable size (MBC, 60–100 μg/ml). Their higher effectiveness is possibly due to the presence of a large number of high-density surface atoms at the corners and edges of the decahedral nanoparticles. The enhanced activity of decahedral AgNPs may also be attributed to the surface charge of the decahedral AgNPs, interfacial atomic arrangements in the crystal, and the crystallographic facets exposed to the environment. This was also supported by zeta potential values where less negative values of zeta potential of decahedral AgNPs may have facilitated higher interaction with the negatively charged bacterial cell surfaces as compared to the citrate-coated spherical AgNPs carrying a higher negative charge. Moreover, increased antibacterial activity of the decahedral AgNPs may also be attributed to more effective interaction due to

the atomic arrangements in the interfaces of the exposed crystal and the crystallographic facets exposed to the surrounding medium as compared to their spherical counterparts, which leads to more effective interaction with the bacterial cell surfaces and enhanced penetration power. The enhanced antibacterial activity of the decahedral AgNPs was not solely due to the slightly higher dissolution of AgNPs to Ag^+ ions. However, the slightly higher silver ion concentration observed for the decahedral AgNPs may also have partly contributed to the higher antibacterial effect. In addition to the surface charge of AgNPs, such interactions are also significantly affected by the surface charge on the bacterial cell surfaces. Thus, the anisotropic silver nanoparticles have substantial potential for use as strong antimicrobials for medical, clinical, and environmental applications.

Supplementary Information The online version contains supplementary material available at https://doi.org/10.1007/s11051-020-05106-z.

Acknowledgments The authors would like to acknowledge the Sophisticated Analytical Instrument Facility (SAIF), IIT Bombay, for providing FEG-TEM, FEG-SEM, and ICP-AES facilities and the Department of Metallurgy Engineering and Materials Science (MEMS), IIT Bombay, for providing the DLS measurement and zeta potential analyzer for characterization of the nanoparticles. The authors would also like to thank Dr. Gauri Shukla for assisting in the preparation of the set-up for photochemical synthesis of decahedral silver nanoparticles.

Authors' contributions Sharda Bharti performed all the experiments, analyzed the results, and prepared the manuscript. Prof. Suparna Mukherji supervised the work and revised the manuscript. Prof. Soumyo Mukherji co-supervised the research work. All authors discussed the experiments and the results and contributed to the final manuscript.

Data availability Not applicable.

Compliance with ethical standards

Conflict of interest The authors declare that they have no conflict of interest.

Ethics approval Not applicable.

Consent to participate Not applicable.

Consent for publication Not applicable.

Code availability Not applicable.

References

Agnihotri S, Mukherji S, Mukherji S (2013) Immobilized silver nanoparticles enhance contact killing and show highest efficacy: elucidation of the mechanism of bactericidal action of silver. Nanoscale 5:7328–7340. https://doi.org/10.1039/C3NR00024A

Agnihotri S, Mukherji S, Mukherji S (2014) Size-controlled silver nanoparticles synthesized over the range 5–100 nm using the same protocol and their antibacterial efficacy. RSC Adv 4:3974–3983. https://doi.org/10.1039/c3ra44507k

Araújo P, Lemos M, Mergulhão F, et al (2011) Antimicrobial resistance to disinfectants in biofilms. In: Science against microbial pathogens: communicating current research and technological advances, A. Méndez-. pp 826–834

Ashbolt NJ (2015) Microbial contamination of drinking water and human health from community water systems. Curr Environ Heal reports 2:95–106

Bae E, Park HJ, Lee J, Kim Y, Yoon J, Park K, Choi K, Yi J (2010) Bacterial cytotoxicity of the silver nanoparticle related to physicochemical metrics and agglomeration properties. Environ Toxicol Chem 29:2154–2160. https://doi.org/10.1002/etc.278

Bharti S, Agnihotri S, Mukherji S, Mukherji S (2015) Effectiveness of immobilized silver nanoparticles in inactivation of pathogenic bacteria. J Environ Res Dev 9:849–856

Casals E, Pfaller T, Duschl A, Oostingh GJ, Puntes V (2010) Time evolution of the nanoparticle protein corona. ACS Nano 4:3623–3632

Chakraborty S, Mukherji S, Mukherji S (2010) Surface hydrophobicity of petroleum hydrocarbon degrading *Burkholderia* strains and their interactions with NAPLs and surfaces. Colloids Surf B: Biointerfaces 78:101–108

Chang S, Chen K, Hua Q, Ma Y, Huang W (2011) Evidence for the growth mechanisms of silver nanocubes and nanowires. J Phys Chem C 115:7979–7986. https://doi.org/10.1021/jp2010088

Cheon JY, Kim SJ, Rhee YH, Kwon OH, Park WH (2019) Shape-dependent antimicrobial activities of silver nanoparticles. Int J Nanomedicine 14:2773–2780. https://doi.org/10.2147/IJN.S196472

Chudasama B, Vala AK, Andhariya N, Upadhyay RV, Mehta RV (2009) Enhanced antibacterial activity of bifunctional Fe_3O_4–Ag core – shell nanostructures. Nano Res 2:955–965. https://doi.org/10.1007/s12274-009-9098-4

Dasgupta N, Ranjan S, Rajendran B et al (2015) Thermal co-reduction approach to vary size of silver nanoparticle: its microbial and cellular toxicology. Environ Sci Pollut Res 23:4149–4163

Dasgupta D, Jasmine J, Mukherji S (2018) Characterization, phylogenetic distribution and evolutionary trajectories of diverse hydrocarbon degrading microorganisms isolated from refinery sludge. 3 biotech 8:1–18. https://doi.org/10.1007/s13205-018-1297-9

El Badawy AM, Silva RG, Morris B et al (2011) Surface charge-dependent toxicity of silver nanoparticles. Environ Sci Technol 45:283–287. https://doi.org/10.1021/es1034188

Franci G, Falanga A, Galdiero S, Palomba L, Rai M, Morelli G, Galdiero M (2015) Silver nanoparticles as potential antibacterial agents. Molecules 20:8856–8874. https://doi.org/10.3390/molecules20058856

Goyal D, Kaur G, Tewari R, Kumar R (2017) Correlation of edge truncation with antibacterial activity of plate-like anisotropic silver nanoparticles. Environ Sci Pollut Res 24:20429–20437. https://doi.org/10.1007/s11356-017-9630-0

Guzmán MG, Dille J, Godet S (2009) Synthesis of silver nanoparticles by chemical reduction method and their antibacterial activity. Int J Chem Biomol Eng 2:104–111

Helmlinger J, Sengstock C, Groß-Heitfeld C, Mayer C, Schildhauer TA, Köller M, Epple M (2016) Silver nanoparticles with different size and shape: equal cytotoxicity, but different antibacterial effects. RSC Adv 6:18490–18501. https://doi.org/10.1039/C5RA27836H

Hong X, Wen J, Xiong X, Hu Y (2016) Shape effect on the antibacterial activity of silver nanoparticles synthesized via a microwave-assisted method. Environ Sci Pollut Res 23:4489–4497. https://doi.org/10.1007/s11356-015-5668-z

Iravani S, Korbekandi H, Mirmohammadi SV, Zolfaghari B (2014) Synthesis of silver nanoparticles: chemical , physical and biological methods. Res Pharm Sci 9:385–406

Ito A, Taniuchi A, May T, Kawata K, Okabe S (2009) Increased antibiotic resistance of *Escherichia coli* in mature biofilms. Appl Environ Microbiol 75:4093–4100. https://doi.org/10.1128/AEM.02949-08

Jose M, Thanal R, Prince Joshua J, Martin Britto Dhas SA, Jerome Das S (2016) Anisotropic growth of silver nanostructures from silver spheres by a simple chemical reduction route. Superlattice Microst 89:68–74. https://doi.org/10.1016/j.spmi.2015.10.039

Keren I, Kaldalu N, Spoering A, Wang Y, Lewis K (2004) Persister cells and tolerance to antimicrobials. FEMS Microbiol Lett 230:13–18. https://doi.org/10.1016/S0378-1097(03)00856-5

Keunen R, Cathcart N, Kitaev V (2014) Plasmon mediated shape and size selective synthesis of icosahedral silver nanoparticles via oxidative etching and their 1-D transformation to pentagonal pins. Nanoscale 6:8045–8051

Lee GP, Shi Y, Lavoie E, Daeneke T, Reineck P, Cappel UB, Huang DM, Bach U (2013) Light-driven transformation processes of anisotropic silver nanoparticles. ACS Nano 7:5911–5921. https://doi.org/10.1021/nn4013059

Li J, Rong K, Zhao H, Li F, Lu Z, Chen R (2013) Highly selective antibacterial activities of silver nanoparticles against *Bacillus subtilis*. J Nanosci Nanotechnol 13:6806–6813. https://doi.org/10.1166/jnn.2013.7781

Li K, Wu Q, Xu T, Kang Q, Yao M, Song G, Lin Y, Chen Z, Zheng T (2016) Silver nanoparticles with different morphologies: growth mechanism and stability. Mater Res Innov 20:58–66. https://doi.org/10.1080/14328917.2015.1130381

Li J, Xie S, Ahmed S, Wang F, Gu Y, Zhang C, Chai X, Wu Y, Cai J, Cheng G (2017) Antimicrobial activity and resistance: influencing factors. Front Pharmacol 8:1–11. https://doi.org/10.3389/fphar.2017.00364

Maillard M, Huang P, Brus L (2003) Silver nanodisk growth by surface plasmon enhanced photoreduction of adsorbed [Ag+]. Nano Lett 3:1611–1615. https://doi.org/10.1021/nl034666d

Mlalila NG, Swai HS, Hilonga A, Kadam DM (2016) Antimicrobial dependence of silver nanoparticles on surface plasmon resonance bands against *Escherichia coli*. Nanotechnol Sci Appl 10:1–9. https://doi.org/10.2147/NSA.S123681

Mohanty S, Mukherji S (2012) Alteration in cell surface properties of Burkholderia spp. during surfactant aided biodegradation of petroleum hydrocarbons. Appl Microbiol Biotechnol 94:193–204

Mukherji S, Ruparelia J, Agnihotri S (2012) Antimicrobial activity of silver and copper nanoparticles: variation in sensitivity across various strains of bacteria and fungi. In: Nano-antimicrobials: progesses and prospects. Springer, Berlin Heidelberg, pp 225–251

Mukherji S, Bharti S, Shukla G, Mukherji S (2018) Synthesis and characterization of size- and shape-controlled silver nanoparticles. Phys Sci Rev 4

Murph SEH, Larsen GK, Coopersmith KJ (2017) Anisotropic and shape-selective nanomaterials: structure-property relationships. Springer International Publishing AG

Murshid N (2013) Controlled transformation of nanoparticles with tunable surface plasmon resonance controlled transformation of nanoparticles with tunable surface plasmon resonance by submitted to the Department of Chemistry. Wilfrid Laurier University

Navaladian S, Viswanathan B, Varadarajan TK, Viswanath RP (2008) Microwave-assisted rapid synthesis of anisotropic Ag nanoparticles by solid state transformation. Nanotechnology 19. https://doi.org/10.1088/0957-4484/19/04/045603

Pal S, Tak YK, Song JM (2007) Does the antibacterial activity of silver nanoparticles depend on the shape of the nanoparticle? A study of the Gram-negative bacterium *Escherichia coli*. Appl Environ Microbiol 73:1712–1720. https://doi.org/10.1128/AEM.02218-06

Pandey PK, Kass PH, Soupir ML et al (2014) Contamination of water resources by pathogenic bacteria. AMB Express 4:1–16

Pencheva D, Bryaskova R, Kantardjiev T (2012) Polyvinyl alcohol/silver nanoparticles (PVA/AgNps) as a model for testing the biological activity of hybrid materials with included silver nanoparticles. Mater Sci Eng C 32:2048–2051

Pietrobon B, Kitaev V (2008) Photochemical synthesis of monodisperse size-controlled silver decahedral nanoparticles and their remarkable optical properties. Chem Mater 20:5186–5190

Pietrobon B, McEachran M, Kitaev V (2009) Synthesis of size-controlled faceted pentagonal silver nanorods with tunable plasmonic properties and self-assembly of these nanorods. ACS Nano 3:21–26. https://doi.org/10.1021/nn800591y

Qi Y, Zhang T, Jing C, Liu S, Zhang C, Alvarez PJJ, Chen W (2020) Nanocrystal facet modulation to enhance transferrin binding and cellular delivery. Nat Commun 11:1–10. https://doi.org/10.1038/s41467-020-14972-z

Rai M, Yadav A, Gade A (2009) Silver nanoparticles as a new generation of antimicrobials. Biotechnol Adv 27:76–83

Raza MA, Kanwal Z, Rauf A, Sabri A, Riaz S, Naseem S (2016) Size- and shape-dependent antibacterial studies of silver nanoparticles synthesized by wet chemical routes. Nanomaterials 6:1–15. https://doi.org/10.3390/nano6040074

Roh J, Umh HN, Sim J, Park S, Yi J, Kim Y (2013) Dispersion stability of citrate- and PVP-coated AgNPs in biological media for cytotoxicity test. Korean J Chem Eng 30:671–674. https://doi.org/10.1007/s11814-012-0172-3

Rojas-Andrade M, Cho AT, Hu P, Lee SJ, Deming CP, Sweeney SW, Saltikov C, Chen S (2015) Enhanced antimicrobial activity with faceted silver nanostructures. J Mater Sci 50: 2849–2858

Ruparelia JP, Chatterjee AK, Duttagupta SP, Mukherji S (2008) Strain specificity in antimicrobial activity of silver and copper nanoparticles. Acta Biomater 4:707–716

Saade J, De Araújo CB (2014) Synthesis of silver nanoprisms: a photochemical approach using light emission diodes. Mater Chem Phys 148:1184–1193. https://doi.org/10.1016/j.matchemphys.2014.09.045

Shannahan JH, Lai X, Ke PC, Podila R, Brown JM, Witzmann FA (2013) Silver nanoparticle protein corona composition in cell culture media. PLoS One 8:e74001. https://doi.org/10.1371/journal.pone.0074001

Silvestry-rodriguez N, Sicairos-ruelas EE, Gerba CP, Bright KR (2007) Silver as a disinfectant. Rev Environ Contam Toxicol 191:23–45. https://doi.org/10.1007/978-0-387-69163-3

Sondi I, Salopek-Sondi B (2004) Silver nanoparticles as antimicrobial agent: a case study on *E. coli* as a model for Gram-negative bacteria. J Colloid Interface Sci 275:177–182

Stamplecoskie K, Scaiano J (2010) Light emitting diode irradiation can control the morphology and optical properties of silver nanoparticles. J Am Chem Soc 8:1825–1827. https://doi.org/10.1021/ja910010b

Valodkar M, Modi S, Pal A, Thakore S (2011) Synthesis and antibacterial activity of Cu, Ag and Cu-Ag alloy nanoparticles: a green approach. Mater Res Bull 46:384–389

Vellora V, Padil T, Černík M (2013) Green synthesis of copper oxide nanoparticles using gum karaya as a biotemplate and their antibacterial application. Int J Nanomedicine:889–898

Xie ZX, Tzeng WC, Huang CL (2016) One-pot synthesis of icosahedral silver nanoparticles by using a photoassisted tartrate reduction method under UV light with a wavelength of 310 nm. ChemPhysChem:2551–2557. https://doi.org/10.1002/cphc.201600257

Yang X, Fu H, Jiang X, Yu A (2013) Silver nanoparticles: synthesis, growth, mechanism and bioapplications. In: Silver nanoparticles: synthesis, Uses and Health Concerns. Nova Science Publishers, Inc., pp 395–460

Yoon KY, Hoon Byeon J, Park JH, Hwang J (2007) Susceptibility constants of *Escherichia coli* and *Bacillus subtilis* to silver and copper nanoparticles. Sci Total Environ 373:572–575. https://doi.org/10.1016/j.scitotenv.2006.11.007

Zhang R, Kang Y, Xie B (2015) Assembly and antibacterial activity of horizontally oriented silver nanoplates. J Appl Polym Sci 132. https://doi.org/10.1002/app.42070

Zheng X, Zhao X, Guo D, Tang B, Xu S, Zhao B, Xu W, Lombardi JR (2009) Photochemical formation of silver nanodecahedra: structural selection by the excitation wavelength. Langmuir 25:3802–3807. https://doi.org/10.1021/la803814j